Routes to spatiotemporal chaos in Kerr optical frequency combs

Aurélien Coillet[1] and Yanne K. Chembo[1, a)]
FEMTO-ST Institute [CNRS UMR6174], Optics Department,
16 Route de Gray, 25030 Besançon cedex, France.

(Dated: 7 January 2014)

We investigate the various routes to spatiotemporal chaos Kerr optical frequency combs obtained through pumping an ultra-high quality whispering-gallery mode resonator with a continuous-wave laser. The Lugiato-Lefever model is used to build bifurcation diagrams with regards to the parameters that are externally controllable, namely, the frequency and the power of the pumping laser. We show that the spatiotemporal chaos emerging from Turing patterns and solitons display distinctive dynamical features. Experimental spectra of chaotic Kerr combs are also presented for both cases, in excellent agreement with theoretical spectra.

arXiv:1401.0927v1 [physics.optics] 5 Jan 2014

Optical Kerr frequency combs are sets of equidistant spectral lines generated through pumping an ultra-high Q whispering gallery mode resonator with a continuous wave laser[1–3]. The Kerr nonlinearity inherent to the bulk resonator induces a four-wave mixing (FWM) process, enhanced by the long lifetime of the intra-cavity photons which are trapped by total internal reflection in the ultra-low loss medium. Four-wave mixing in this context allows for the creation and mixing of new frequencies as long as energy and momentum conservation laws are respected[4,5]. These Kerr combs are the spectral signatures of the dissipative spatiotemporal structures arising along the azimuthal direction of the disk-resonator. When the resonator is pumped in the anoumalous group-velocity dispersion regime, various spatiotemporal patterns can can build up, namely, Turing patterns, bright and dark solitons, breathers, or spatiotemporal chaos[6–8]. In this work, we investigate the evolution of the Kerr combs towards spatiotemporal chaos when the frequency and the pump power of the laser are varied. We evidence the key bifurcations leading to these chaotic states and also discuss chaotic Kerr comb spectra obtained experimentally, which display excellent agreement with their numerical counterparts.

I. INTRODUCTION

It was recently shown in refs.[9–11] that Kerr comb generation can be efficiently modelled using the Lugiato-Lefever equation[12], which is a nonlinear Schrödinger equation with damping, detuning and driving. This partial differential equation describes the dynamics of the complex envelope of the total field inside the cavity.

Spatiotemporal chaos is generally expected to arise in spatially extended nonlinear systems when they are submitted to a strong excitation. In the context of Kerr combs generation, such chaotic states have been evidenced theoretically in ref.[4] using a modal expansion method, which allowed to demonstrate that the Lyapunov exponent is positive under certain circumstances. The experimental evidence of these chaotic states was provided in the same reference, and has been analyzed in other works as well[13]. In the present article, we are focusing on the routes leading to spatiotemporal chaos. To the best of our knowledge, the bifurcation scenario to chaos in this system is to a large extent unexplored, despite the dynamical richness of this system.

The plan of the article is the following. In the next section, we present the experimental system and the model used to investigate its nonlinear dynamics. A brief overview of the various dissipative structures is presented in Sec. III. The following section is devoted to the route to chaos based on the destabilization of Turing patterns, while Sec. V is focused on the second route which relies on the destabilization of cavity solitons. The experimental results are presented in Sec. VI, and the last section concludes the article.

II. THE SYSTEM

The system under study consists of a sharply resonant whispering-gallery mode cavity made of dielectric material, pumped with a continuous-wave laser (see Fig. 1). The coupled resonator can be characterized by its quality factor $Q = \omega_0/\Delta\omega$ where $\Delta\omega$ is the spectral linewidth of the (loaded) resonance at the angular frequency ω_0 of the resonance. Typical values for Q-factors leading to the generation of Kerr combs are in the range of 10^9. In WGM resonators, the eigenmodes of the fundamental family are quasi-equidistant, and

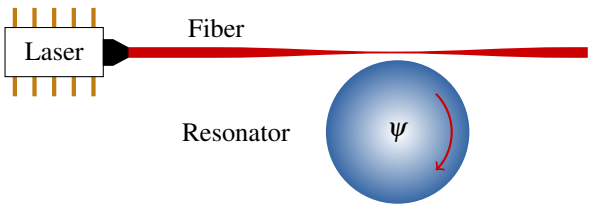

FIG. 1. Schematic representation of the Kerr comb generator. Continuous laser light is coupled into a ultra-high Q whispering gallery-mode resonator using a tapered fiber. Inside the cavity, and above a certain threshold power, the four-wave mixing induced by the Kerr nonlinearity can excite several eigenmodes, thereby leading to a chaotic spatiotemporal distribution of the intra-cavity optical field.

a)Electronic mail: yanne.chembo@femto-st.fr

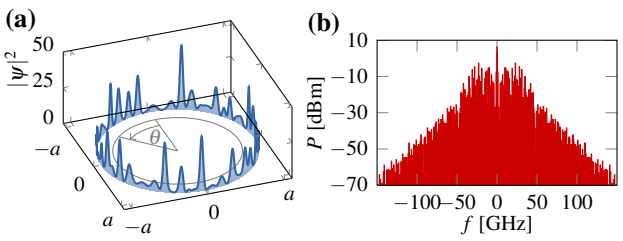

FIG. 2. (a) 3D representation of the simulated optical intensity inside the WGM resonator. In the chaotic regime, peaks of various amplitudes arise and disappear in the cavity. (b) Corresponding optical spectrum. This spectrum is made of discrete and quasi-equidistant spectral lines, and for this reason, is generally referred to as a Kerr optical frequency comb.

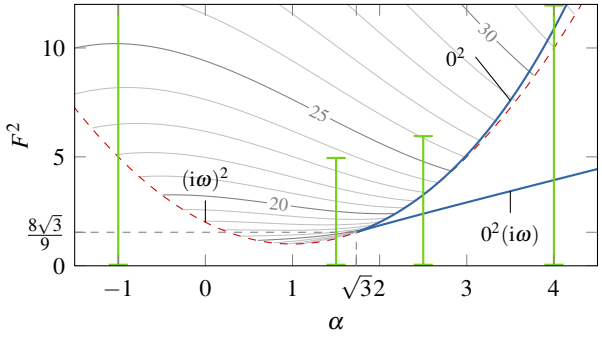

FIG. 3. Stability diagram of the Lugiato-Lefever equation for $\beta < 0$ in the α-F^2 plane[8]. In between the two blue lines, three flat solutions exist while only one is found outside this area. The red dashed lines corresponds to the flat solution $|\psi|^2 = 1$. Characteristic bifurcations can be associated to each of these curves. Note that the green lines vertical segments correspond to the bifurcation diagrams simulated in Figs. 4 and 5. The thin gray curves indicate the number of rolls contained in the cavity when the system is in the Turing pattern regime.

these modes can be excited by the pump excitation above a certain threshold.

Kerr comb generation in high-Q whispering-gallery mode resonators can be described by two kinds of models. The first kind describes the evolution of each resonant mode in the cavity, producing a system of N ordinary differential equations, with N being the number of modes to be taken into consideration[4,5]. While this modal model allows for the easy determination of comb generation threshold, its computational cost makes it inappropriate for studying the evolution towards chaos of the system. Furthermore, only a finite, arbitrary number of modes can be simulated with this model which reduces the accuracy of the numerical results, especially for chaotic systems where a very large number of modes is excited. While the modal description consisted in large set of ordinary differential equations, the spatiotemporal formalism provides an unique partial differential equation ruling the dynamics of the full intracavity fieldrefs.[9–11]. From the numerical point of view, this latter description allows for easy and fast simulations using the split-step Fourier algorithm, thus allowing the construction of bifurcation diagrams in order to study the mechanisms that lead to chaos in a highly resonant and nonlinear optical cavity.

In its normalized form, the LLE describing the spatiotemporal dynamics of the intracavity field ψ explicitly reads[10]

$$\frac{\partial \psi}{\partial \tau} = -(1+i\alpha)\psi + i|\psi|^2\psi - i\frac{\beta}{2}\frac{\partial^2 \psi}{\partial \theta^2} + F \qquad (1)$$

where $\tau = t/2\tau_{\mathrm{ph}}$ is a dimensionless time ($\tau_{\mathrm{ph}} = 1/\Delta\omega$ being the photon lifetime) and θ is the azimuthal angle along the circumference of the disk-resonator. The real-valued and dimensionless parameters of the equation are the laser frequency detuning α, the second-order dispersion β, and the laser pump field F. The link between these dimensionless parameters and the physical features of the real system are explicitly discussed in refs.[6,10].

Chaos preferably arises in the system in the regime of anomalous dispersion, which corresponds to $\beta < 0$ (see refs.[5,8]). It is also important to note that the two parameters of the system that can be controlled experimentally are related to the pump signal. In particular, the laser pump power is proportional to F^2, and will be the scanned parameter of our bifurcation diagrams. Intuitively, it can be understood that the more energy is coupled inside the cavity, the more frequencies will be created through the Kerr-induced four-wave mixing, ultimately leading to chaotic behavior. The other parameter accessible to the experiments is the detuning frequency α between the pump laser and the resonance. It is expressed in terms of modal linewidths, in the sense that $\alpha = -2(\Omega_0 - \omega_0)/\Delta\omega$ where Ω_0 and ω_0 are the laser and resonance angular frequencies, respectively.

At the experimental level, the most easily accessible characteristic of the system is its optical spectrum. Effectively, while the LLE model rules the dynamics of the spatiotemporal variable ψ, the spectrum can be obtained by performing the Fourier transform of the optical field in the cavity. This duality is illustrated on Fig. 2, and we will use it to compare our numerical simulations to the experimental results.

III. DISSIPATIVE STRUCTURES

A stability analysis of the LLE in the α-F^2 plane of parameters has shown that various regimes of Kerr combs can be observed depending on the detuning and pump power[8]. Figure 3 represents this α-F^2 plane where the spatial stability domain and bifurcations lines of the stationary solutions have been drawn. This diagram shows that the value $\alpha = \sqrt{3}$ is of particular interest, and we will address the two cases $\alpha < \sqrt{3}$ and $\alpha > \sqrt{3}$ separately.

On the one hand, for detunings α below $\sqrt{3}$, the LLE only has one constant ("flat") solution for $\psi(\tau, \theta)$. It has previously been shown in ref.[8] that this constant solution becomes (modulationally) unstable when the external pump F^2 reaches a threshold value $F^2_{\mathrm{th}} = 1 + (\alpha - 1)^2$, and Turing patterns (rolls) are formed. Due to the periodicity of the variable θ, only integer numbers of rolls can be found in the cavity, and a

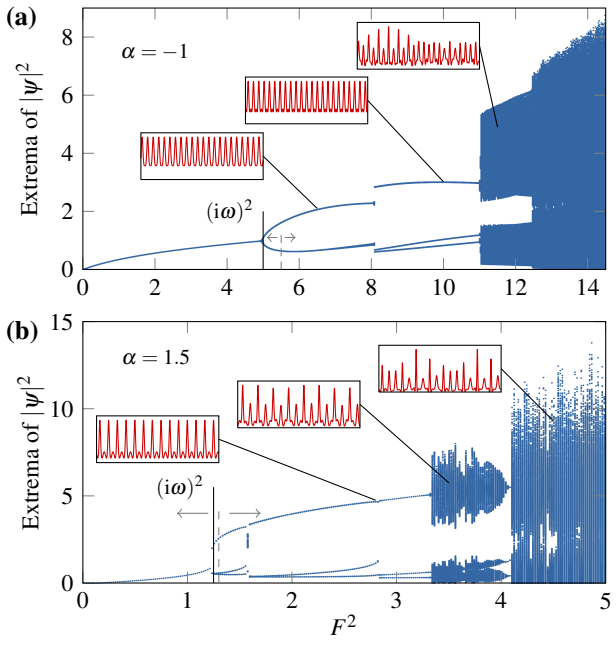

FIG. 4. Bifurcation diagram in the case $\alpha = -1$ (a) and $\alpha = 1.5$ (b). In both cases, the initial condition is a small noisy background just above the bifurcation $(\mathrm{i}\omega)^2$. This first bifurcation leads to the formation of Turing patterns, number of rolls given by 2. While the excitation is increased, these rolls become unstable and one or several more rolls appear abruptly in the cavity. For higher gain, the amplitudes of the peaks oscillate, and finally, a chaotic regime is reached. Note that the inserts (in red) are snapshots displaying $|\psi|^2$ in a range $[-\pi, \pi]$.

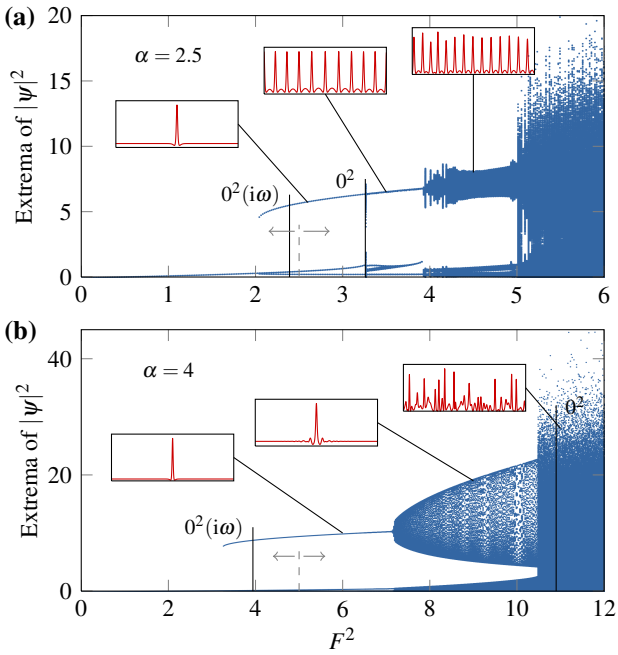

FIG. 5. Bifurcation diagram in the cases $\alpha = 2.5$ (a) and $\alpha = 4$ (b). In both cases the initial condition is chosen such that an unique soliton is present in the cavity for excitations just above the $0^2(\mathrm{i}\omega)$ bifurcation. When the 0^2 bifurcation is quickly reached (case $\alpha = 2.5$), the soliton remains stable until this bifurcation. At that point, other peaks are created that fill entirely the cavity. For higher F^2, their amplitudes vary in time, and finally, spatiotemporal chaos occurs. In the case $\alpha = 4$, the 0^2 bifurcation happens at much higher excitations, and the soliton becomes unstable and bifurcates to a breather characterized by a temporally fluctuating amplitude. The system becomes chaotic in the vicinity of the 0^2 bifurcation. The inserts (in red) are snapshots displaying $|\psi|^2$ in a range $[-\pi, \pi]$.

close approximation of this number is given at threshold by

$$l_{\mathrm{th}} = \sqrt{2(\alpha - 2)/\beta}. \tag{2}$$

The iso-value lines for the rolls in the α-F^2 plane are displayed in the bifurcation diagram of Fig. 3.

On the other hand, when α is greater than $\sqrt{3}$, one to three constant solutions can be found depending on the value of F^2. It is also in this area of the plane that solitary waves can be found, such as cavity solitons or soliton breathers. Unlike the previous case of Turing patterns, solitons always need an appropriate initial condition to be excited.

In order to investigate the route towards chaos in this two cases, numerical simulations were performed using the split-step Fourier method. The value for the loaded quality factor was such that $Q = 10^9$, and a slightly negative dispersion parameter was considered ($\beta = -0.0125$). The evolution of the optical field in the cavity is simulated from the initial condition and for a duration of 1 ms, which is more than one hundred times longer than the photon lifetime $\tau_{\mathrm{ph}} = Q/\omega_0$. The extrema of the 100 last intensity profiles are recorded and plotted as a function of the excitation F^2, thereby yielding bifurcation diagrams. In the next sections, we present the results for the numerical simulations of the LLE in these two different regimes.

IV. DESTABILIZATION OF TURING PATTERNS

In the $\alpha < \sqrt{3}$ region of the bifurcation diagram, the starting point of the bifurcation diagram simulations is a noisy background while the pump power is above the threshold. In this condition, the flat solution is unstable if the bifurcation diagram specifically starts at a value $\alpha < 41/30$, and the noise allows the system to evolve toward stable rolls in the cavity. After 1 ms of simulation, the pump power is increased and the system is simulated again, the previous final state being the initial condition. In order to draw the lower part of the diagram, the same methodology is used, starting from the same initial point. The resulting diagrams are presented in Fig. 4, for $\alpha = -1$ and 1.5.

The $(\mathrm{i}\omega)^2$ bifurcation appears clearly in this diagrams, and corresponds to the apparition of super-critical Turing patterns when $\alpha < 41/30$ and sub-critical Turing patterns when $\alpha > 41/30$ (see refs.[6,8,12]). At this point, the number of rolls in the cavity is given by Eq. (2) and Fig. 3 gives the values of l above threshold. However, after further increase of the excitation, the number of rolls in the cavity may not correspond to

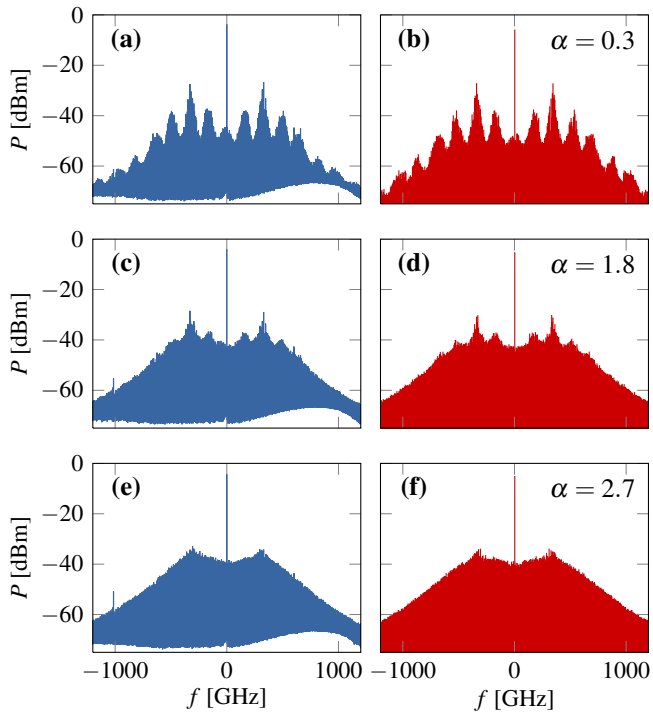

FIG. 6. Experimental (left, a, c and e) and simulated (right, b, d and f) Kerr combs obtained at same pump power and different detunings. Excellent agreement is observed between experimental and theoretical results. The frequency f is relative to the laser frequency. This frequency was decreased (α increased) between the spectra (a), (c) and (e) while the pump power remained unchanged (around 300 mW). The numerical simulations were performed with $F^2 = 12$, $\beta = 2.2 \times 10^{-3}$ and $\alpha = 0.3$ for the (b) case, $\alpha = 1.8$ for (d) and $\alpha = 2.7$ for (f). While the first spectra (a) and (b) clearly arise from destabilized Turing patterns (note the spectral modulation), the last sets spectra originate from the destabilization of cavity solitons.

this ideal number, and the pattern changes abruptly when the number of rolls has to shift. This phenomenon is responsible for the discontinuities observed on the bifurcation diagrams.

For very high excitation, the Turing patterns become unstable, starting with oscillations in the amplitude of the rolls' peaks. These fluctuations become stronger as F^2 is increased, finally leading to a chaotic behavior with peaks of diverse amplitudes.

V. DESTABILIZATION OF SOLITONS

In the case $\alpha > \sqrt{3}$, the initial condition is chosen such that the system converges to an unique soliton located at $\theta = 0$. At this point, the bifurcation diagram shows three extrema corresponding to the soliton maximum, the continuous background and the dips on each side of the soliton (pedestals).

Since the soliton is a sub-critical structure[6,10,12] linked to a $0^2(i\omega)$ bifurcation[8], it is still present for F^2 just below the bifurcation value, as shown on Fig. 5. When the excitation is increased, the soliton maintains its qualitative shape, with the continuous background being increased while the dips remains approximately at the same level.

When the 0^2 bifurcation is reached, the previously stable continuous background becomes unstable, and the soliton can no longer be unique: a train of identical pulses whose shapes are similar to the initial soliton appear in the cavity. These pulses fill entirely the cavity, in a similar fashion to what was observed in the $\alpha < \sqrt{3}$ case.

For relatively small detunings, the subsequent evolution of the bifurcation diagram is similar to the $\alpha < \sqrt{3}$ case, with fluctuations of the pulses amplitudes ultimately leading to a chaotic repartition of the energy in the cavity. For greater detunings ($\alpha = 4$ in Fig 5), the 0^2 bifurcation happens at very high excitations, and the soliton remains alone in the cavity for a large range of pump power F^2. This soliton becomes unstable in the process, and transforms into a soliton breather whose peak amplitude oscillates periodically with time. The amplitude of the oscillations increases with F^2 until the system explodes to chaos in the vicinity of the 0^2 bifurcation.

VI. EXPERIMENTAL SPECTRA

In the experimental setup, a continuous-wave laser beam is amplified and coupled to a WGM resonator using a bi-conical tapered fiber, as portrayed in Fig. 1. The output signal is collected at the other end of the same fiber and monitored either in the spectral domain with a high-resolution spectrum analyzer, or in the temporal domain with a fast oscilloscope. It should be noted that this output signal is the sum of both the continuous pump signal and the optical field inside the cavity: the measured spectra will only differ from the intra cavity spectra through an increased contribution from the pump laser.

The WGM resonator is made of magnesium fluoride (MgF_2) with refraction index $n_0 = 1.37$ at 1550 nm. This dielectric bulk material has been chosen for two reasons. First, this crystal is characterized by very low absorption losses, allowing for ultra-high Q-factors, equal to 2×10^9 (intrinsic) in our case. Secondly, the second-order dispersion of MgF_2 is anomalous at the pumping telecom wavelength ($\lambda = 1550$ nm), so that the waveguide dispersion is not strong enough to change the regime dispersion; the overall dispersion generally remains anomalous regardless of the coupling. The diameter of the WGM resonator is $d \sim 11.3$ mm and its free-spectral range (FSR – also referred to as *intermodal frequency*) is $\Delta\omega_{FSR}/2\pi = c/\pi n_0 d = 5.8$ GHz, where c is the velocity of light in vacuum.

Once an efficient coupling is achieved, the pump power is increased to few hundreds of milliwatts, and the detuning is adjusted so that Kerr frequency combs are generated. Further adjustments of these two parameters allow us to reach chaotic regimes where every mode of the fundamental family in the WGM resonator is populated. In the example of Figs. 6(a), (c) and (e), the pump power was fixed and the detuning was changed from a negative value to a positive value by increasing the wavelength. The bump in the background noise level is due to the unfiltered amplified spontaneous emission (ASE) originating from the optical amplifier

used in the experiment. The comb (a) corresponds to a destabilized Turing pattern where the so-called primary and secondary combs[5] have evolved by populating nearby modes until every mode is filled. On the contrary, the structure of spectrum (e) is smooth, and originates from the destabilization of cavity solitons. The comb presented in (c) stands in the transition between the two different regimes. In each case however, important fluctuations of the amplitude of each mode are observed, confirming the chaotic nature of these experimental Kerr combs. To obtain representative spectra, the (a), (c) and (e) spectra were averaged over 30 consecutive measurements.

In Fig. 6, we also provide numerical simulations of the optical spectra that qualitatively correspond to their experimental counterparts. The dispersion parameter was determined using Eq. (2) and an experimental spectra with Turing patterns near threshold, yielding $\beta = 2.2 \times 10^{-3}$.

Similarly to the experiments, the simulated combs were obtained for a fixed pump power $F^2 = 12$ and three different detunings. The first one, $\alpha = 0$ correspond to the Turing pattern case while the last one $\alpha = 2.7$ is in the soliton regime. The transition case was taken for $\alpha = 1.8$, close to the $\alpha = \sqrt{3}$ limit. As stated previously, the power of the central mode has been increased with 11.5 dBm to account for the differences between the intra-cavity and output spectra. To simulate the integration of the spectrum analyzer, the spectra are averaged over the last 1000 iterations. The agreement between numerical simulations and experiments is excellent: it covers an impressive dynamical range of 80 dB, and a spectral range of 2 THz which corresponds to more than 300 modes. This agreement also validates the interpretation of these combs as the result of two different routes to spatiotemporal chaos.

VII. CONCLUSION

In this work, we have investigated the generation of optical Kerr combs in WGM resonators using the Lugiato-Lefever equation to describe our experimental system. Numerical simulations allowed us to draw bifurcation diagrams of the system for various frequency detuning values. The natural scanning parameter in this case is the pump power injected in the resonator. Depending on the value of the detuning parameter, various routes to chaos have been evidenced. In particular, for detunings α below $\sqrt{3}$, the chaotic Kerr combs originate from destabilized Turing patterns. In this case, the envelope of the corresponding Kerr comb displays several maxima which are reminiscent of the primary and secondary combs encountered at lower excitation. For α higher than $\sqrt{3}$, the evolution of a soliton can either lead to a set of unstable pulses filling the cavity or optical breathers before reaching chaos. The optical spectrum in this case is smooth, with a shape similar to the soliton's spectrum. In both cases, the numerical spectra are in excellent agreement with the experimental results obtained using a ultra-high Q magnesium fluoride resonator, thereby providing a strong validation of the model and simulations.

ACKNOWLEDGMENTS

The authors acknowledge financial support from the European Research Council through the project NextPhase (ERC StG 278616).

[1] T. J. Kippenberg, S.M. Spillane, and K. J. Vahala, Phys. Rev. Lett. **93**, 083904 (2004).
[2] A. A. Savchenkov, A. B. Matsko, D. S. Strekalov, M. Mohageg, V. S. Ilchenko, and L. Maleki, Phys. Rev. Lett. **93**, 243905 (2004).
[3] P. Del'Haye, A. Schliesser, A. Arcizet, R. Holzwarth, and T. J. Kippenberg, *Nature* **450**, 1214 (2007).
[4] Y. K. Chembo, D. V. Strekalov, and N. Yu, Phys. Rev. Lett. **104**, 103902 (2010).
[5] Y. K. Chembo and N. Yu, Phys. Rev. A **82**, 033801 (2010).
[6] A. Coillet, I. Balakireva, R. Henriet, K. Saleh, L. Larger, J. M. Dudley, C. R. Menyuk, and Y. K. Chembo, *IEEE Phot. J.* **5**, 6100409 (2013).
[7] C. Godey, I. Balakireva, A. Coillet, and Y. K. Chembo, arXiv:1308.2539 (2013).
[8] I. Balakireva, A. Coillet, C. Godey, and Y. K. Chembo, arXiv:1308.2542 (2013).
[9] A. B. Matsko, A. A. Savchenkov, W. Liang, V. S. Ilchenko, D. Seidel, and L. Maleki, Opt. Lett. **36**, 2845 (2011).
[10] Y. K. Chembo and C. R. Menyuk, Phys. Rev. A **87**, 053852 (2013).
[11] S. Coen, H. G. Randle, T. Sylvestre, and M. Erkintalo, Opt. Lett. **38**, 37 (2013).
[12] L. A. Lugiato and R. Lefever, Phys. Rev. Lett. **58**, 2209 (1987).
[13] A. B. Matsko, W. Liang, A. A. Savchenkov, and L. Maleki, *Opt. Lett.* **38**, 525 (2013).